

Dipole and quadrupole Cooper minima and their effects on dipole and nondipole photoelectron angular distributions in Hg 6s

T. Banerjee and P. C. Deshmukh*

Department of Physics, Indian Institute of Technology, Madras, Chennai 600 036, India

S. T. Manson

Department of Physics and Astronomy, Georgia State University, Atlanta, Georgia 30303, USA

(Received 15 December 2006; revised manuscript received 16 March 2007; published 6 April 2007)

A theoretical study of dipole and quadrupole Cooper minima, along with dipole and nondipole photoelectron angular distribution parameters, in Hg 6s has been performed using the relativistic-random-phase approximation methodology. It is found that the Cooper minima affect the angular distribution parameters dramatically. In addition, the results show that the angular distribution parameters are extremely sensitive to both relativistic and correlation effects (interchannel coupling).

DOI: [10.1103/PhysRevA.75.042701](https://doi.org/10.1103/PhysRevA.75.042701)

PACS number(s): 32.80.Fb, 31.25.Jf

I. INTRODUCTION

Up to about 5 keV above the ionization threshold, integrated photoionization cross sections are described rather well by the dipole approximation [1,2]. With developments in instrumental precision and brighter light sources, however, it has been found that even at much lower energy, hundreds or even tens of eV, differential cross sections (photoelectron angular distributions) require the inclusion of higher-order terms in r/λ , thereby including higher multipoles in the description of photoionizing transitions. Investigation of these higher-order terms has attracted considerable recent attention from both experimentalists and theorists [3–10]. These angular distribution studies provide information on quadrupole photoionization amplitudes, information that is difficult to get in other ways. In addition, the photoelectron angular distribution parameters depend upon ratios of matrix elements, rather than on absolute squares of matrix elements like the integrated cross section. Thus, angular distributions are much more sensitive to the effect(s) of correlation and relativistic interactions on the various amplitudes, particularly the small ones, as compared to the integrated cross section. They are also much more sensitive to the location of Cooper minima [11] in both dipole ($E1$) and quadrupole ($E2$) channels. The locations of these Cooper minima are, in turn, extremely sensitive to electron-electron correlation and relativistic effects.

The ns states in a closed-shell system provide an ideal laboratory to study both relativistic effects and correlation. For ns states, deviation of the dipole angular distribution asymmetry parameter β from the value 2 in a closed-shell system can occur only because of relativistic effects, since transition amplitudes to relativistic $p_{3/2}$ and $p_{1/2}$ continuum channels differ. No amount of interchannel coupling or other correlation within a nonrelativistic framework can cause β to deviate from 2. Furthermore, the dependence of the nondipole angular distribution asymmetry parameter γ on the dipole and quadrupole transition matrix elements is rather

simple (much simpler than for np , nd , or nf subshells), so the relationship of the matrix elements to the nondipole behavior is easily understood.

As a means of studying these various effects, the dipole and nondipole photoelectron angular distribution parameters of the valence 6s state of atomic mercury has been investigated in the present work. This choice was dictated by a number of factors. First, it is an ns state which simplifies interpretation of the results as discussed above. Second, Hg is heavy enough so that relativistic effects play a non-negligible role, even in the valence shell. Third, the Hg 6s $E1$ channel exhibits two Cooper minima, and it was expected that there would be at least one $E2$ Cooper minimum as well. Fourth, correlation in the form of interchannel coupling was found to be very important in an earlier calculation. Finally, Hg offers the possibility of experimental investigation of the phenomena investigated in this paper.

Dipole photoionization parameters in atomic mercury have been studied previously in the energy range from the 6s ionization threshold up to about 45 eV [12–16] above threshold. Experimental results have been found to be in reasonably good agreement with the theoretical predictions of relativistic random-phase approximation (RRPA) [17], relativistic time-dependent local density approximation [18], and relativistic time-dependent density functional theory [19] calculations. The previous RRPA study [17] of Hg 6s photoionization was restricted to the photon energy range from 0.65 a.u. (16.69 eV) up to 2.5 a.u. (68.03 eV), and the RRPA was truncated to include interchannel coupling with ionization channels only from the 6s and 5d subshells. This study predicted that there are two minima in the 6s dipole photoionization cross section, recognized as the Cooper minima, one below the 5d threshold, and another above the energy range that was investigated, but the actual positions of these minima were not determined.

In the present work, the earlier dipole RRPA calculation [17] is extended in energy range and the number of interacting channels, along with the inclusion of $E2$ (quadrupole) photoionization channels. Computations of 6s photoionization parameters of atomic mercury have been carried out using the RRPA methodology. The calculations have been

*Electronic address: pcd@physics.iitm.ac.in

performed at various levels of truncation, i.e., including various levels of correlation in the form of interchannel coupling, in order to investigate the role these correlation effects play in both dipole and quadrupole photoionizing transitions, since these correlations are known to be of importance in other systems [7,8,20]. Of particular interest is the effect of interplay of relativistic and correlation effects on various $E1$ and $E2$ photoionization parameters in a system as heavy as Hg. Specifically, the present study focuses on the $E1$ (dipole) and $E2$ (quadrupole) parameters β_{6s} and γ_{6s} , which are strongly dependent on the positions of the $E1$ and $E2$ Cooper minima. To our knowledge, the present work is the first study of $E2$ transitions from a heavy atom taking into account both correlation and relativistic effects. In addition, this is the first investigation of an $E2$ photoionization in which interchannel coupling with channels arising from nf photoionizing transitions is taken into account.

Within the framework of the dipole approximation, the photoelectron angular distribution for a subshell i is completely specified by the parameter β_i . Beyond the dipole approximation, however, inclusion of the next order term (neglecting $M1$ transitions which are negligibly small [21]) necessitates the consideration of two additional angular distribution parameters due to the interference of $E1$ and $E2$ terms. The differential cross section for photoionization is then given by [23]

$$\frac{d\sigma_i}{d\Omega} = \frac{\sigma_i}{4\pi} [1 + \beta_i P_2(\cos \theta) + (\delta_i + \gamma_i \cos^2 \theta) \sin \theta \cos \phi], \quad (1)$$

where σ_i is the angle-integrated cross section, β_i is the dipole angular distribution anisotropy parameter which arises from $E1$ - $E1$ interference terms, and δ_i and γ_i are nondipole asymmetry parameters which arise from $E1$ - $E2$ interference terms; θ and ϕ are the polar coordinates of the photoelectron momentum vector \vec{p} in a coordinate system with photon polarization vector along the z axis and photon propagation vector along the x axis. For an ns subshell, δ_i is negligible [21].

As is well known, many important electron correlation effects are built into RRPA [24–27]. The RRPA takes into account correlations in both initial and final (interchannel coupling) states on an equal footing by including both time backward ring diagrams (to include initial-state correlations) and time-forward ring diagrams (to include final-state interchannel coupling correlations). These correlations affect the energy-dependent dynamical profiles of photoabsorption parameters. The RRPA, however, does not include two electron excitations from a given subshell to final states having different orbital angular momenta. When the latter correlations are of importance, results of the RRPA are usually not quite satisfactory [19]. Within the framework of the RRPA [25,27] the electron correlations in the initial and final states are built up on Dirac-Fock (DF) reference states. Some non-RPA correlations can be accounted for by using the experimental thresholds instead of the Dirac-Fock thresholds. While the experimental thresholds are available for some of the outermost subshells of atomic mercury, in our RRPA calculations

TABLE I. Dirac-Fock and experimental [29] ionization thresholds for atomic Hg.

Subshell	Threshold in eV	
	DF	Experimental [29]
6s	8.9263	10.4301
5d _{5/2}	15.6372	14.8411
5d _{3/2}	17.6894	16.7011
5p _{3/2}	77.3342	71.5659
5p _{1/2}	96.2716	90.3418
5s	138.8621	133.9888
4f _{7/2}	117.3288	107.1856
4f _{5/2}	121.7154	110.9952
4d _{5/2}	382.3932	
4d _{3/2}	402.6430	
4p _{3/2}	603.7871	
4p _{1/2}	710.8782	
4s	833.9892	

we have used the DF ionization thresholds. The DF and the experimental [28,29] ionization thresholds are listed in Table I.

The calculations were performed using the dipole and quadrupole RRPA codes of Johnson and co-workers [21,25] to calculate the RRPA dipole and quadrupole matrix elements and their phases, along with the dipole photoelectron angular distribution parameter β_i . The nondipole parameters were calculated using our own code, using the output of the RRPA codes as input.

II. DIPOLE PHOTOIONIZATION PARAMETERS

The calculations of the 6s dipole photoionization of Hg were carried out using differing levels of truncation of the RRPA methodology, i.e., including differing levels of interchannel coupling effects, as a means of ascertaining the contribution of the various interchannel couplings to the photoabsorption process. It is well known that as a result of truncation, the agreement between the results in length and velocity gauges [30] is lost; nevertheless, in our calculations, the disagreement typically is not larger than 5%. In the present work, $E1$ parameters have been computed at the following levels of truncation: (1) two $E1$ channels from the 6s subshell; (2) eight $E1$ channels from the 6s and 5d subshells; and 34 $E1$ channels from the 6s, 5d, 5p, 5s, 4f, 4d, 4p, and 4s subshells.

At the lowest level of truncation, the results in the two-channel case, which includes only intrashell coupling between the 6s channels, are presented in Figs. 1 and 2. In Fig. 1(a)–1(c) are presented the 6s photoionization cross sections, the vertical scale of Fig. 1(c) being magnified compared to Figs. 1(a) and 1(b) to highlight the local minima. Also shown in Fig. 1(a) are the partial $E1$ cross sections for the 6s $\rightarrow \epsilon p_{3/2}$ and 6s $\rightarrow \epsilon p_{1/2}$ photoionization channels included in the RRPA intrashell coupling. Figure 2 shows the dipole an-

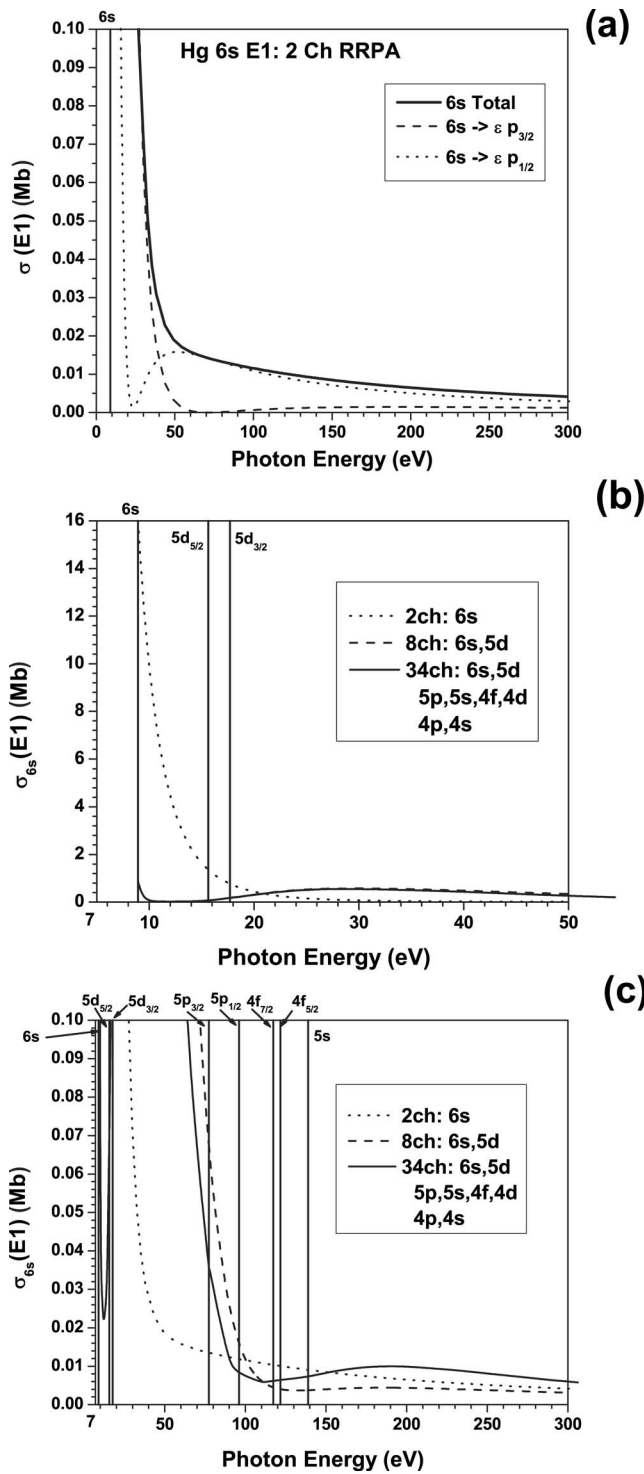


FIG. 1. (a) Hg 6s dipole cross section σ and $6s \rightarrow \epsilon p_{3/2}$ and $6s \rightarrow \epsilon p_{1/2}$ partial cross sections resulting from the two-channel coupling of RRPA calculation. (b) Hg 6s dipole cross section σ at three levels of truncation of RRPA coupling: (i) 6s, (ii) 6s and 5d, (iii) 6s, 5d, 5p, 5s, 4f, 4d, 4p and 4s, from the 6s ionization threshold up to 50 eV. (c) Hg 6s dipole cross section σ at three levels of truncation of the RRPA coupling: (i) 6s, (ii) 6s and 5d, (iii) 6s, 5d, 5p, 5s, 4f, 4d, 4p, and 4s from the 6s ionization threshold up to 300 eV with an expanded vertical scale. Vertical lines indicate the ionization threshold energies for the various subshells of atomic Hg.

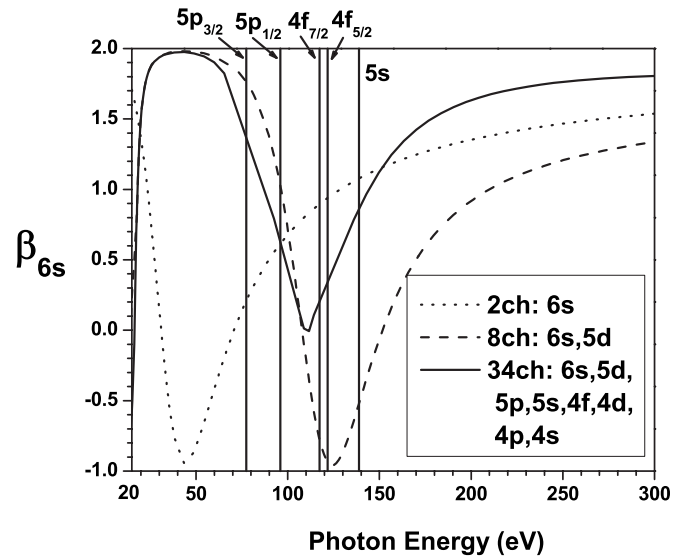


FIG. 2. Hg 6s dipole angular distribution asymmetry parameter β at the three levels of truncation of the RRPA, coupling channels from (i) 6s, (ii) 6s and 5d, (iii) 6s, 5d, 5p, 5s, 4f, 4d, 4p, and 4s, from 20 eV (above 5d ionization thresholds). Vertical lines indicate the ionization threshold energies for the various subshells of atomic Hg.

gular distribution asymmetry parameter β_{6s} . It is seen that the $6s \rightarrow \epsilon p_{3/2}$ and $6s \rightarrow \epsilon p_{1/2}$ matrix elements go through Cooper minima [11,31] at ~ 69 and ~ 23 eV, respectively [Fig. 1(a)]. The $6s \rightarrow \epsilon p_{1/2}$ matrix element goes through its Cooper minimum at a lower photon energy than the $6s \rightarrow \epsilon p_{3/2}$ channel, since the spin-orbit interaction for $j=l-\frac{1}{2}$ is attractive whereas it is repulsive for $j=l+\frac{1}{2}$. This makes the continuum final-state $\epsilon p_{1/2}$ wave function more compact than the $\epsilon p_{3/2}$ wave function, making the zero in the $6s \rightarrow \epsilon p_{1/2}$ matrix element occur at a somewhat lower energy than the zero in the $6s \rightarrow \epsilon p_{3/2}$ channel. The fact that the $j=l-\frac{1}{2}$ minimum occurs at a lower photon energy than the $j=l+\frac{1}{2}$ is known to be a general phenomenon in the relativistic splitting of Cooper minima [32]. Note also that the minimum value of the $6s \rightarrow \epsilon p_{1/2}$ partial cross section is not as low as the minimum value of the $6s \rightarrow \epsilon p_{3/2}$ partial cross section. This is due to the fact that the $6s \rightarrow \epsilon p_{3/2}$ matrix element is about a factor of 40 larger than the $6s \rightarrow \epsilon p_{1/2}$ matrix element at the energy of the $6s \rightarrow \epsilon p_{1/2}$ Cooper minimum, and interchannel coupling (intrashell in this case) drives the $6s \rightarrow \epsilon p_{1/2}$ oscillator strength. On the other hand, at the energy at which the $6s \rightarrow \epsilon p_{3/2}$ channel goes through its Cooper minimum, the $6s \rightarrow \epsilon p_{1/2}$ strength is relatively small; consequently, the $6s \rightarrow \epsilon p_{3/2}$ goes through a near-zero value because the interchannel coupling is not very important in this case. The total 6s cross section itself, however, does not show any local minima; it decreases monotonically since the Cooper minima in the two channels occur at dramatically different energies, and one channel dominates the cross section when the other channel goes through its Cooper minimum.

The angular distribution asymmetry parameter β_{6s} is seen to go to a value of -1 at ~ 42 eV, between the Cooper minima in the two channels. Nonrelativistically, for a closed-

shell atom, the angular distribution asymmetry parameter β_{ns} for an ns subshell is always equal to 2. However, in a relativistic analysis, the single $s \rightarrow p$ channel splits into two channels, $ns \rightarrow \epsilon p_{3/2}$ and $ns \rightarrow \epsilon p_{1/2}$, and this causes β_{ns} to depart from its nonrelativistic value of 2 depending on the differences in the relativistic amplitudes in the two channels. The relativistic expression for β_{ns} for an ns subshell in a closed-shell atom is given by [27,33]

$$\beta_{ns}(\omega) = 2 - \frac{3|A_T(\omega)|^2}{|A_S(\omega)|^2 + |A_T(\omega)|^2} \quad (2)$$

where $A_T(\omega)$ and $A_S(\omega)$ are the dipole matrix elements corresponding to the final continuum triplet and singlet states of Hg, respectively. In terms of the radial dipole matrix elements for the $ns \rightarrow \epsilon p_{3/2}$ and $ns \rightarrow \epsilon p_{1/2}$, $R_{3/2}$ and $R_{1/2}$, respectively, the expression for β_{ns} is given as [34]

$$\beta_{ns}(\omega) = \frac{2R_{3/2}(\omega)^2 + 4R_{1/2}(\omega)R_{3/2} \cos(\delta_{1/2} - \delta_{3/2})}{R_{1/2}(\omega)^2 + 2R_{3/2}(\omega)^2} \quad (3)$$

with $\delta_{1/2}$ and $\delta_{3/2}$ the phases of the respective dipole matrix elements. From this equation it is evident that β_{ns} should take on values of 0 and 1 at the $p_{3/2}$ and $p_{1/2}$ Cooper minima, respectively, and that is exactly what is seen in Fig. 2. In addition, between the Cooper minima, β_{ns} takes on the value of -1 at ~ 42 eV. From the above equation, at this energy the dipole matrix elements have opposite signs and the magnitude of the $p_{3/2}$ matrix element is twice that of $p_{1/2}$.

At the next level of truncation of the RRPA, in addition to photoionization channels from the $6s$ subshell, channels from the relativistically split $5d_{5/2}$ and $5d_{3/2}$ subshells are coupled. As a result of this, the Cooper minima in the $6s$ $E1$ channels move to lower photon energy, in fact, below the $5d_{3/2}$ threshold in the region of the $5d \rightarrow nf$, np autoionization resonances. These resonances dominate the cross section from the $6s$ threshold up to the $5d_{3/2}$ threshold (8.9–17.7 eV). The fact that the $6s$ Cooper minima are shifted to energies below the $5d_{3/2}$ threshold is nevertheless borne out by the fact that the angular distribution asymmetry parameter β is seen to rise toward a value of 2 above the $5d_{3/2}$ threshold, as seen in the ($6s, 5d$) coupled result in Fig. 2, dramatically different from the two-channel result. The RRPA provides a natural framework to study the autoionization resonances since interchannel coupling between open and closed channels is built into the methodology. Nevertheless, the autoionization resonances are studied more efficiently using a combination of the RRPA and the relativistic multichannel quantum defect theory (RMQDT) [35]. The RMQDT studies will be reported separately. For the present, we estimate that the position of the $p_{1/2}$ Cooper minimum is about 14.5 eV and the $p_{3/2}$ is at roughly 17 eV, in agreement with earlier predictions [17], i.e., the energy of the $p_{1/2}$ Cooper minimum is lowered by about 8.5 eV and the $p_{3/2}$ by an astounding 52 eV, owing to the interchannel coupling of the $6s$ photoionization channels with the $5d$ channels. This shows that the interchannel coupling completely changes the character of the dipole transitions from Hg $6s$. This is a manifestation of a general phenomenon; when two nearby channels are degenerate, interchannel coupling modifies the weaker channel [31]. In

this case, the $5d$ cross section is approximately a factor of 50 larger than the $6s$ cross section, so that the $6s$ matrix element is significantly altered.

But that is not the whole story; interchannel coupling between $6s$ and $5d$ channels induces a second set of Cooper minima in the $6s$ photoionization channels, seen in the cross sections shown in Fig. 1. The minima in the individual channels (not shown) are at ~ 100 eV and ~ 150 eV for $p_{1/2}$ and $p_{3/2}$, respectively. These minima are reflected in the second dip toward -1 in the value of β , shown in Fig. 2 where β is seen to take on the values of 1 and 0 at the minima, as indicated by Eq. (3).

For the highest level of truncation considered, all 34 relativistic photoionization channels down to the $4s$ channels, the situation remains essentially the same as in the eight-channel case as far as the low-energy Cooper minima and β are concerned. This is to be expected since, of the 26 new channels considered, the closest in energy are from $5p_{3/2}$, which opens at just above 77 eV. Thus, looking at the situation perturbatively, there is a large energy denominator in the interchannel coupling matrix element with the $5p_{3/2}$ and higher channels, which renders their effect on the $6s$ photoionization amplitudes in the 10–20 eV region negligible. Figures 3 show the cross section and angular distribution asymmetry parameter β , computed using the RRPA at the highest level of truncation (34 coupled channels) in the low-energy region from $6s$ ionization threshold up to 40 eV. Below the $5d$ thresholds, where autoionization resonances are important, the results have been averaged over the resonances.

It was reported in [15] that the Cooper minimum in $6s$ dipole photoionization is at about 20 eV, above the $5d$ ionization thresholds, whereas the present 34-channel RRPA results shows a Cooper minimum below $5d$ ionization thresholds, as Fig. 3(a) displays clearly. The angular distribution parameter in Fig. 3(b) shows a deviation from 2.0 in this energy range, which confirms the existence of the Cooper minimum below the $5d$ thresholds. These differences with [15], which corresponds to the present eight-channel results, are clearly due to the differing levels of truncation of the two RRPA calculations.

Although the lower-energy Cooper minima are not significantly affected by coupling with the channels arising from subshells more tightly bound than the $5d$, the situation is otherwise for the higher-energy Cooper minima that were induced by interchannel coupling with the $5d$ channels. The additional interchannel coupling from subshells $5p$, $5s$, $4f$, $4d$, $4p$, and $4s$ (mainly due to coupling of channels from the $5p$, $5s$, and $4f$ subshells which open in the 80–120 eV range) shifts the higher-energy $p_{3/2}$ minimum by about 25 eV (lower) to about 125 eV, while the lower-energy $p_{1/2}$ minimum remains at roughly the same energy as the eight-channel case. Significant interchannel coupling, caused by the newly opened channels that are much stronger than $6s$ [36], is clearly manifested by the energy shift of the higher-energy $p_{3/2}$ minimum and the marked increase in the minimum value of the magnitude of the dipole matrix element in the case of the $p_{1/2}$ minimum. This increased magnitude at the minimum occurs because the interchannel coupling renders the matrix element complex, and the real and imaginary

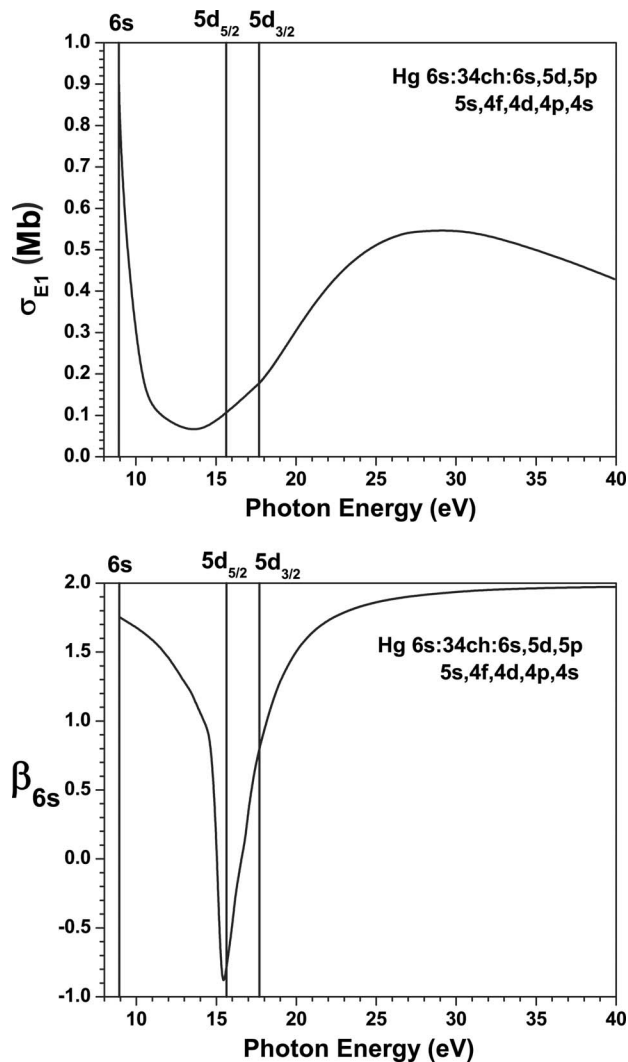


FIG. 3. Hg 6s dipole cross section and angular distribution asymmetry parameter β in the RRPA, coupling all the $E1$ channels from 6s, 5d, 5p, 5s, 4f, 4d, 4p, and 4s, from the 6s ionization threshold up to 40 eV. Vertical lines indicate the ionization threshold energies for the various subshells of atomic Hg.

parts go through zeros at differing energies, thereby causing the minimum value of the matrix element to be nonzero; the further apart the real and imaginary zeros are, the greater the magnitude at the minimum. Note that the increase in the 34-channel 6s cross section relative to the eight-channel result above the higher-energy Cooper minimum in the 125–300 eV energy region, seen in Fig. 1(c), is due primarily to interchannel coupling with the very strong 4f photoionization channels. This is evident because the 6s cross section mirrors the shape of the 4f cross section in this energy region.

Owing to these changes in the high-energy pair of Cooper minima, resulting from the extra interchannel coupling included in the 34-channel calculation, the value of the β parameter is altered accordingly. Since the minima are closer together than in the eight-channel case, the dip in β is correspondingly narrowed. In addition, since the dipole matrix elements no longer are very close to zero at the Cooper

minima, the simple analysis that explained the two-channel and eight-channel cases is not entirely applicable at the 34-channel level. The β parameter drops only to about zero, rather than -1 , between the minima in this case. This behavior is similar to what is known about β for Xe 5s near threshold [34] and is symptomatic of strong interchannel coupling. The somewhat nonsmooth behavior of β in the 34-channel case is due to the autoionizing resonance that occur below each of the five thresholds in the 77–121 eV energy range. Note that the 4d, 4p, and 4s channels have virtually no effect upon the 6s channels in the photon energy range up to 300 eV, shown in Fig. 1. This is because they open at much higher energies, so the interchannel coupling matrix element is quite small, owing to the large energy denominator. It follows then that the channels arising from still more deeply bound subshells will have even less influence on the 6s amplitudes in the energy region below 300 eV. Thus, the results presented are essentially equivalent to what would be obtained from the RRPA calculation with no truncation at all.

III. QUADRUPOLE PHOTOIONIZATION PARAMETERS

Using exactly the same methodology and philosophy applied to the study of the dipole photoelectron angular distribution β parameter, calculations have been performed at the following levels of truncation for quadrupole ($E2$) photoionization of mercury 6s: (1) two $E2$ channels from the 6s subshell; (2) 11 $E2$ channels from the 6s and 5d subshells; and (3) 46 $E2$ channels from the 6s, 5d, 5p, 5s, 4f, 4d, 4p, and 4s subshells.

At the lowest level of truncation, the two intrashell $E2$ channels $6s \rightarrow \epsilon d_{3/2}$ and $6s \rightarrow \epsilon d_{5/2}$ are coupled. The partial cross sections for these two channels, along with the total 6s $E2$ cross section, are shown in Fig. 4(a) where the occurrence of a pair of quadrupole Cooper minima [37] is revealed in the ~ 120 eV energy region, one in each of the relativistic $6s \rightarrow \epsilon d$ channels. The individual $6s \rightarrow \epsilon d_{5/2}$ and $6s \rightarrow \epsilon d_{3/2}$ quadrupole channels are seen to go through their respective Cooper minima at ~ 124 and ~ 106 eV in the two-channel calculation. The total 6s cross section, the sum of these two channels, is seen to display a rather pronounced minimum at about 115 eV. The overall scale of this quadrupole cross section is seen to be considerably smaller than the comparable dipole cross section.

The quadrupole angular distribution asymmetry parameter γ is determined by the interference between the $E1$ and the $E2$ channels. Specifically, γ is given by the ratio of $E2$ to $E1$ matrix elements, scaled by the cosine of the difference between the phase shifts of the $E1$ and the $E2$ channels. γ is a linear function of the $E2$ matrix elements, whereas σ varies as the square of $E2$ matrix elements. The matrix elements being very small, the $E2$ cross section is not easy to measure. However, since γ involves the ratios of matrix elements, it is very sensitive to the energy dependence of the matrix elements, and γ is amenable to laboratory investigation. The (relativistic) expression for the nondipole parameter γ for an initial ns state of a closed-shell atom is obtained from [22] with a modicum of angular momentum algebra as

$$\gamma = \frac{3\alpha\omega 6R_{3/2}^{(1)}(\omega)R_{3/2}^{(2)}(\omega)\cos\Delta_{3/2,3/2} + 5R_{1/2}^{(1)}(\omega)R_{5/2}^{(2)}(\omega)\cos\Delta_{1/2,5/2} + 4R_{3/2}^{(1)}(\omega)R_{5/2}^{(2)}(\omega)\cos\Delta_{3/2,5/2}}{5R_{1/2}^{(1)}(\omega)^2 + 2R_{3/2}^{(1)}(\omega)^2}, \quad (4)$$

where α is the fine structure constant, ω is the photon energy, $R_j^{(1)}$ and $R_{j'}^{(2)}$ are the dipole ($E1$) and quadrupole ($E2$) radial matrix elements, and $\Delta_{j,j'}$ is the difference between $\delta_{\epsilon p_j}$ and $\delta_{\epsilon d_{j'}}$, the phase shifts of the ϵp_j and $\epsilon d_{j'}$ continuum functions, respectively. In an energy region where there are no Cooper minima, the matrix elements and phase shifts are independent of j , to an excellent approximation. Under such circumstances, the expression for γ for s states reduces to the nonrelativistic result [23]

$$\gamma = 3\alpha\omega \frac{R^{(2)}(\omega)}{R^{(1)}(\omega)} \cos(\delta_{\epsilon p} - \delta_{\epsilon d}). \quad (5)$$

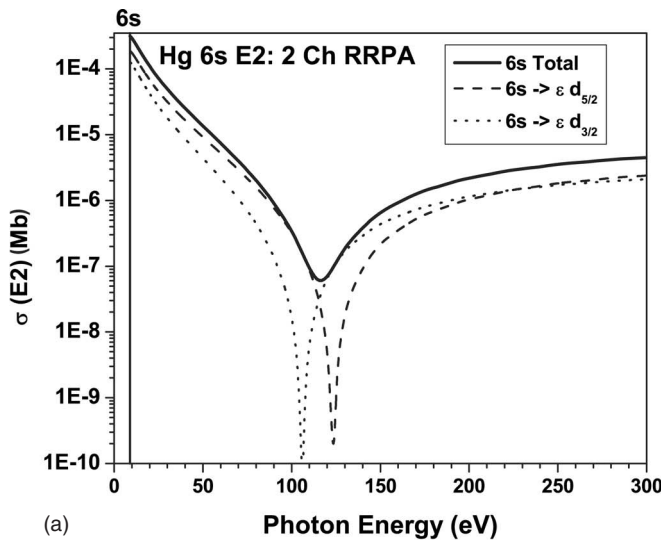
From Eqs. (4) and (5) it is seen that the γ parameter has an energy dependence that is significantly influenced by the Cooper minima in the dipole and quadrupole channels, along with the cosine terms. At the Cooper minima in the dipole channels, γ becomes large, and at the Cooper minima in the quadrupole channels, γ tends to go to zero. Nonrelativistically, the ratio of the quadrupole $6s \rightarrow \epsilon d$ matrix element to the dipole $6s \rightarrow \epsilon p$ matrix element goes through a local maximum at the position of the $E1$ Cooper minimum, and becomes zero at the $E2$ Cooper minimum, modulated by the cosine function in Eq. (5). However, this simple nonrelativistic analysis provides only general pointers to the dynamics that affect the nondipole angular distribution, considering the fact that dipole and quadrupole Cooper minima are each split into a pair of minima through the influence of relativistic interactions so that in the region of Cooper minima (dipole or quadrupole), it is Eq. (4) that applies.

The γ parameter resulting from the combination of the two-channel dipole calculation with the two-channel quadrupole calculation is shown in Fig. 5. This 2-channel γ parameter shows a low-energy maximum in the neighborhood of 30 eV, reflecting the effects of the low-energy dipole Cooper minima which were seen to be situated in this region. Above these energies, the behavior of the low-energy two-channel γ parameter is dominated by the cosine term; the resulting oscillatory behavior is quite evident. Since the two-channel quadrupole cross section has Cooper minima in the 115 eV region, γ should be close to zero in that region; this is exactly what is seen in Fig. 5. Note, however, that γ also goes through a zero at about 45 eV. Thus, although quadrupole Cooper minima imply a zero value of γ , a zero value of γ does not necessarily imply quadrupole Cooper minima. In addition, this case shows the importance of including relativistic effects in the calculations involving high- Z elements; without the relativistic splitting of the dipole Cooper minimum, the low-energy γ parameter would exhibit qualitatively different behavior—a much more significant (and unphysical) low-energy maximum.

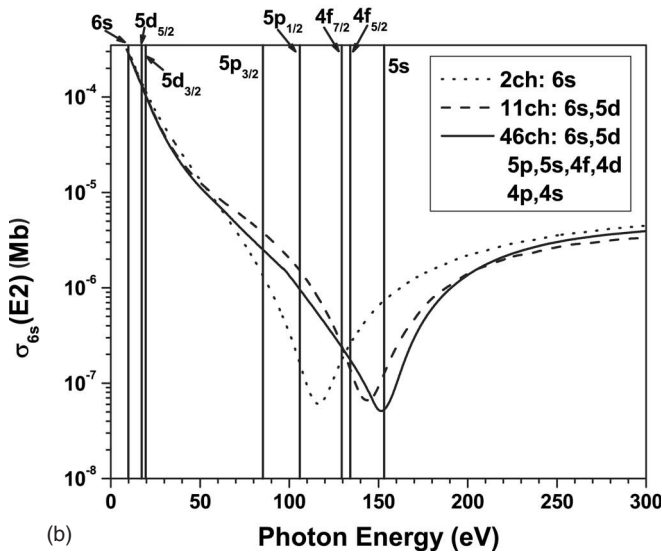
For the intermediate, $6s$ and $5d$ 11-coupled-channel calculation, the results are rather different, indicating a strong interchannel coupling effect of the $5d$ quadrupole channels on the $6s$ channels. The quadrupole cross section, presented in Fig. 4(b), shows that the Cooper minima have moved to larger energy, in fact about 30 eV larger, to the 145 eV region. The individual minima (not shown) are located at ~ 150 and ~ 135 eV, a significant shift to higher photon energies from the two-channel case. Unlike the dipole case, however, the relativistic splitting of the minima is not significantly affected by the $5d$ coupling. Far away from the quadrupole Cooper minima, the 11-channel quadrupole cross section is seen in Fig. 4(b) to be substantially the same as the two-channel result.

The resulting γ parameter, using both quadrupole and dipole results that include coupling only among $6s$ and $5d$ photoionization channels, is shown in Fig. 5, where it is seen to be rather different from the two-channel result; below the opening of the $5d$ channels the results have been smoothed through the resonance region. Clearly, interchannel coupling is an important effect here. The low-energy behavior is rather different, owing to a number of factors—the resonances, the alteration of the low-energy dipole Cooper minima by the interchannel coupling, the fact that the interchannel coupling makes the matrix elements (both dipole and quadrupole) complex and the real and imaginary parts go through their respective Cooper minima at differing energies so that the Cooper minima are shallower, and the change in the relative phases engendered by the interchannel coupling. At the higher energies, the quadrupole Cooper minima in the 145 eV region lead to a zero in γ in that region, i.e., the zero induced by the quadrupole Cooper minima has moved to higher energy by the amount that the quadrupole Cooper minima have been shifted by the interchannel coupling. At still higher energy, the 11-channel γ is seen to tend to the two-channel result, indicating that the interchannel coupling with the $5d$ channels is not so important at these higher energies.

For the most extensive calculation, coupling all nl single-ionization channels for $n=4, 5$, and 6, the 46-channel quadrupole cross section is shown in Fig. 4(b), and it is not so very different from the 11-channel result, i.e., the interchannel coupling of the $6s$ channels with channels from $5p$ down to $4s$ is not so large. Of the new couplings in this 46-channel case, only coupling with the $4f$ channels seems to have any significant effect, and the quadrupole cross-section minimum moves out another 5 eV to about 150 eV, as seen in Fig. 4(b). The actual quadrupole Cooper minima (not shown) are at ~ 156 and ~ 142 eV in the 46-channel calculation. Note that there are resonances below each of the inner-shell thresholds, but the cross section presented has been smoothed over these resonances; the resonance regions will be dealt with in a future study. In any case, the 46-channel



(a)



(b)

FIG. 4. (a) Hg 6s quadrupole cross section σ and $6s \rightarrow \epsilon d_{5/2}$ and $6s \rightarrow \epsilon d_{3/2}$ partial cross sections on a logarithmic scale resulting from the two-channel RRPA calculation in the photon energy range from the 6s ionization threshold up to 300 eV. (b) Hg 6s cross section σ on a logarithmic scale at three levels of truncation of the RRPA, coupling channels from (i) 6s, (ii) 6s and 5d, and (iii) 6s, 5d, 5p, 5s, 4f, 4d, 4p, and 4s in the photon energy region from the 6s ionization threshold up to 300 eV.

results being the most accurate, the (smoothed) quadrupole cross section is presented in detail in the lower-energy region in Fig. 6(a).

The γ parameter for this most extensively coupled case is shown in Fig. 5, and it is seen to be rather similar to the intermediate 6s plus 5d case in the low-energy region. At the higher energies there is some shift to higher energy of the 46-channel γ as compared to the 11-channel prediction, primarily as a result of the shift of the quadrupole Cooper minima to higher energy owing to the additional interchannel coupling. The γ parameter goes through a zero at about 150 eV, owing to these quadrupole Cooper minima. A detailed view of the 46-channel low-energy γ parameter is

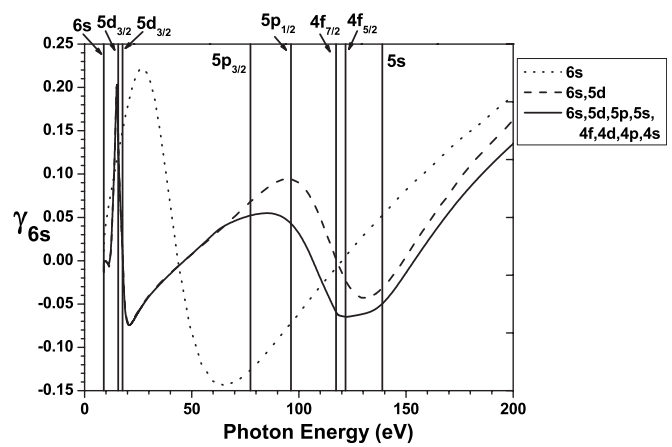


FIG. 5. Hg 6s nondipole angular distribution asymmetry parameter γ at three levels of truncation of the RRPA, coupling channels from (i) 6s, (ii) 6s and 5d, (iii) 6s, 5d, 5p, 5s, 4f, 4d, 4p, and 4s from the 6s ionization threshold. Vertical lines indicate the ionization threshold energies for different subshells of atomic Hg.

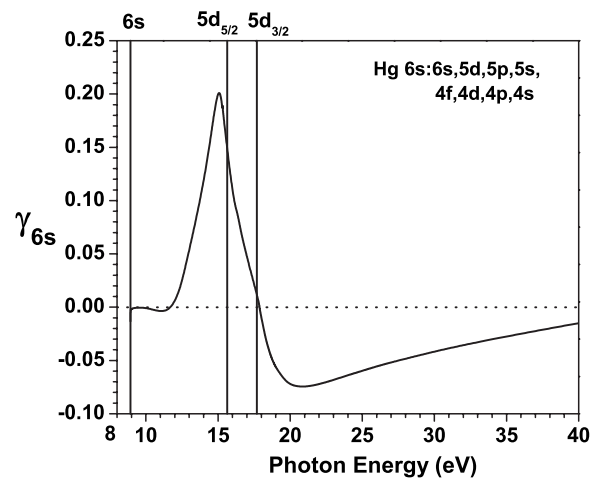
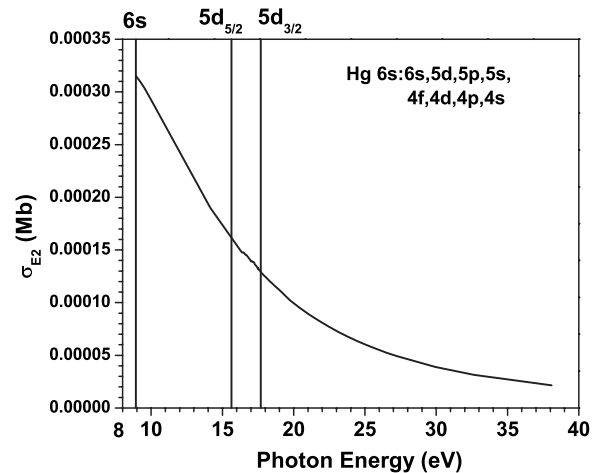


FIG. 6. Hg 6s quadrupole cross section and nondipole angular distribution asymmetry parameter γ in the RRPA, coupling all the channels from 6s, 5d, 5p, 5s, 4f, 4d, 4p, and 4s from the 6s ionization threshold up to 40 eV. Vertical lines indicate the ionization threshold energies for the various subshells of atomic Hg.

given in Fig. 6(b) and shows the low-energy maximum in γ that results from the low-energy dipole Cooper minima.

IV. CONCLUSIONS

Photoelectron angular distributions, both dipole and non-dipole (quadrupole), are significantly influenced by both relativistic and interchannel coupling effects. Cooper minima in the dipole and the quadrupole channels affect the energy dependence of the angular distribution of the photoelectrons strongly, and the details are very sensitive to electron correlations arising out of interchannel coupling in both dipole and quadrupole manifolds. It is expected that many of the

findings of the present investigation are applicable to other high- Z atoms as well. Finally, since the closed-shell mercury atom is experimentally tractable, we hope that the present study will stimulate measurements of the dipole and nondipole angular distribution asymmetry parameter resulting from the photoionization of atomic mercury.

ACKNOWLEDGMENTS

This work was partially supported by BRNS, DAE, and DST (India) along with DOE, Basic Energy Sciences, and NSF (U.S.A.). The authors are grateful to Walter Johnson for valuable discussions and for the use of his RRPA codes.

-
- [1] H. A. Bethe and E. E. Salpeter, *Quantum Mechanics of One- and Two-electron Atoms* (Springer, Berlin, 1957).
- [2] M. Ya. Amusia, A. S. Baltenkov, A. A. Grinberg, and S. G. Shapiro, *Zh. Eksp. Teor. Fiz.* **68**, 28 (1975) [*Sov. Phys. JETP* **41**, 14 (1975)]; M. Ya. Amusia and N. A. Cherepkov, *Case Studies in Atomic Physics* (North-Holland, Amsterdam, 1975), Vol. 5, p. 155.
- [3] B. Krässig, M. Jung, D. S. Gemmell, E. P. Kanter, T. LeBrun, S. H. Southworth, and L. Young, *Phys. Rev. Lett.* **75**, 4736 (1995).
- [4] M. Jung, B. Krässig, D. S. Gemmell, E. P. Kanter, T. LeBrun, S. H. Southworth, and L. Young, *Phys. Rev. A* **54**, 2127 (1996).
- [5] O. Hemmers, G. Fisher, P. Glans, D. L. Hansen, H. Wang, S. B. Whitefield, R. Wehlitz, J. C. Levin, I. A. Sellin, R. C. C. Perera, E. W. B. Dias, H. S. Chakraborty, P. C. Deshmukh, S. T. Manson, and D. W. Lindle, *J. Phys. B* **30**, L727 (1997).
- [6] W. R. Johnson and K. T. Cheng, *Phys. Rev. A* **63**, 022504 (2001).
- [7] O. Hemmers, R. Guillemin, E. P. Kanter, B. Krässig, D. W. Lindle, S. H. Southworth, R. Wehlitz, J. Baker, A. Hudson, M. Lotrakul, D. Rolles, W. C. Stolte, I. C. Tran, A. Wolska, S. W. Yu, M. Ya. Amusia, K. T. Cheng, L. V. Chernysheva, W. R. Johnson, and S. T. Manson, *Phys. Rev. Lett.* **91**, 053002 (2003).
- [8] O. Hemmers, R. Guillemin, D. Rolles, A. Wolska, D. W. Lindle, K. T. Cheng, W. R. Johnson, H. L. Zhou, and S. T. Manson, *Phys. Rev. Lett.* **93**, 113001 (2004).
- [9] D. W. Lindle and O. Hemmers, *J. Electron Spectrosc. Relat. Phenom.* **100**, 297 (1999).
- [10] O. Hemmers, R. Guillemin, and D. W. Lindle, *Radiat. Phys. Chem.* **70**, 123 (2004).
- [11] J. W. Cooper, *Phys. Rev.* **128**, 681 (1962).
- [12] S. P. Shannon and K. Codling, *J. Phys. B* **11**, 1193 (1978).
- [13] J. L. Dehmer and J. Berkowitz, *Phys. Rev. A* **10**, 484 (1974).
- [14] B. H. Mc Quaide, M. S. Banna, P. Gerard, and M. O. Krause, *Phys. Rev. A* **35**, 1603 (1987).
- [15] F. Schäfers, Ch. Heckenkamp, M. Müller, V. Radojević, and U. Heinzmann, *Phys. Rev. A* **42**, 2603 (1990).
- [16] M. Zubek, D. B. Thompson, P. Bolognesi, D. Cooper, and G. C. King, *J. Phys. B* **38**, 1657 (2005).
- [17] W. R. Johnson, V. Radojević, P. C. Deshmukh, and K. T. Cheng, *Phys. Rev. A* **25**, 337 (1982).
- [18] F. A. Parpia and W. R. Johnson, *J. Phys. B* **16**, L375 (1983).
- [19] D. Toffoli, M. Stener, and P. Decleva, *Phys. Rev. A* **66**, 012501 (2002).
- [20] H. Wang, G. Snell, O. Hemmers, M. M. Sant'Anna, I. Sellin, N. Berrah, D. W. Lindle, P. C. Deshmukh, N. Haque, and S. T. Manson, *Phys. Rev. Lett.* **87**, 123004 (2001).
- [21] A. Derevianko, W. R. Johnson, and K. T. Cheng, *At. Data Nucl. Data Tables* **73**, 153 (1999).
- [22] W. R. Johnson, A. Derevianko, K. T. Cheng, V. K. Dolmatov, and S. T. Manson, *Phys. Rev. A* **59**, 3609 (1999).
- [23] J. W. Cooper, *Phys. Rev. A* **42**, 6942 (1990); **47**, 1841 (1993).
- [24] A. Dalgarno and G. A. Victor, *Proc. R. Soc. London, Ser. A* **291**, 291 (1966).
- [25] W. R. Johnson and C. D. Lin, *Phys. Rev. A* **20**, 964 (1979).
- [26] T. N. Chang and U. Fano, *Phys. Rev. A* **13**, 263 (1976).
- [27] W. R. Johnson, C. D. Lin, K. T. Cheng, and C. M. Lee, *Phys. Scr.* **21**, 409 (1980).
- [28] M. Kutzner, C. Tidwell, S. E. Vance, and V. Radojević, *Phys. Rev. A* **49**, 300 (1994).
- [29] H. Siegbahn and L. Karlsson, in *Corpuscles and Radiation in Matter*, edited by W. Mehlhorn, *Handbuch der Physik* Vol. 31 (Springer-Verlag, Berlin, 1982), p. 215.
- [30] D. L. Lin, *Phys. Rev. A* **16**, 600 (1977).
- [31] U. Fano and J. W. Cooper, *Rev. Mod. Phys.* **40**, 441 (1968).
- [32] P. C. Deshmukh, B. R. Tambe, and S. T. Manson, *Aust. J. Phys.* **39**, 679 (1986).
- [33] P. C. Deshmukh and S. T. Manson, *Phys. Rev. A* **28**, 209 (1983).
- [34] T. E. H. Walker and J. T. Waber, *J. Phys. B* **7**, 674 (1974).
- [35] C. M. Lee and W. R. Johnson, *Phys. Rev. A* **22**, 979 (1980).
- [36] P. H. Kobrin, P. A. Heimann, H. G. Kerkhoff, D. W. Lindle, C. M. Truesdale, T. A. Ferrett, U. Becker, and D. A. Shirley, *Phys. Rev. A* **27**, 3031 (1983).
- [37] M. S. Wang and R. H. Pratt, *Phys. Rev. A* **29**, 174 (1984).